

Ingredients for enhanced thermoelectric power at cryotemperatures in the correlated semiconductor CoSbS revealed by its optical response

R. Yang^{1,*}, M. Corasaniti^{1,*}, L. Wu², Q. Du^{2,3,†}, Y. Zhu², C. Petrovic^{2,3} and L. Degiorgi¹

¹Laboratorium für Festkörperphysik, ETH-Zürich, 8093 Zürich, Switzerland

²Condensed Matter Physics and Materials Science Department, Brookhaven National Laboratory, Upton, New York 11973, USA

³Department of Materials Science and Chemical Engineering, Stony Brook University, Stony Brook, New York 11790, USA



(Received 5 January 2021; accepted 12 April 2021; published 23 April 2021)

Semiconducting CoSbS is well known for its thermoelectric performance at high temperatures but it is also of interest because of its colossal low-temperature thermopower. Here, we address the temperature dependence of its optical response over a broad spectral range, from which we reveal several ingredients determining the thermoelectric properties at cryotemperatures. We discover coherent phonon modes and with the additional support of scanning transmission electron microscopy investigations we provide evidence for in-gap impurity states driving the formation of correlated electrons in the valence band. Their implications, with respect to the high thermoelectric power at low temperatures, are discussed within the framework of the phonon-drag transport of low-mobility heavy quasiparticles.

DOI: [10.1103/PhysRevB.103.L161111](https://doi.org/10.1103/PhysRevB.103.L161111)

Converting heat (mostly of waste nature) into electric power (and vice versa) is nowadays attracting great interest and is at the center of novel and sustainable green and carbon-neutral technologies for power generation [1–3]. This demands the development of efficient thermoelectric materials for which the thermopower Seebeck coefficient S , and the electrical (σ) and thermal (κ) conductivities supportively conspire in order to enhance the well-known figure of merit $zT = (S^2\sigma/\kappa)T$ (T being the temperature). The ideal scenario would consist in being able to enhance S and/or σ , together with a reduction of κ [1,4]. One can immediately realize that this is a quite challenging endeavor, since the Wiedemann-Franz law requires the electronic part of the thermal conductivity to be proportional to the electrical one [5]. Therefore, innovative strategies in order to seek an optimal balance among those relevant parameters were intensively searched. A key strategy exploits semiconducting materials with an appropriately well-designed electronic structure for which an overwhelming enhancement of S over the phonon thermal conductivity can be implemented. A colossal Seebeck effect in high-purity semiconductors with ballistic phonons [6,7] and a considerable reduction of the thermal conductivity by phonon coherence in nanostructures and nanomaterials [8] are just two possible avenues.

Besides the obvious technological interest in thermoelectric materials at high T , some efforts have been recently devoted to scrutinize opportunities for thermoelectric cryo-devices. Such cryothermoelectric materials provide an arena for the study of the additional interplay between electronic correlations, which cannot be neglected at cryogenic T , and

the thermopower factor ($S^2\sigma$) as well as the thermal conductivity. In this context, PbTe is an emblematic example, since Tl substitution for Pb yields a metallic state, with no carrier freeze-out to the lowest T , and a superconducting ground state for Tl concentrations above $x_c \sim 0.3\%$ [9,10]. From the overall optical response of Tl-doped PbTe, it clearly emerges that the effective optical mass m^*/m_e is the key quantity, showing a strong enhancement for $x > x_c$ [11]. The enhancement of m^*/m_e originates from the formation of resonant impurity states [12] and advances in principle the intriguing possibility that superconductivity may be a consequence of the pairing of “heavy” quasiparticles via quantum valence fluctuations [13], even underlining some Kondo-like physics in thermoelectric materials [14]. The concept of a sharp peak in the density of states (DOS) originating from narrow bands near the Fermi level (ϵ_F) because of electronic correlations was originally introduced by Mahan and Sofo [15] as a complementary yet alternative approach to the optimization of the phonon transport in order to boost the thermopower.

Other promising materials are FeSb₂ and CoSbS, which nicely allow one to establish a link between thermoelectric properties and phonon transport as well as correlated charge carriers. Indeed, the former displays a low- T colossal Seebeck effect [16], related to substantial electron-electron correlations [17] or enhanced by phonons dragging massive electrons [18]. The title compound also exhibits a giant low- T thermopower consistent with the accumulation of heavy electrons at the semiconducting gap edges [19]. While the buildup of electronic correlations on cooling in semiconducting CoSbS may be understood within a Kondo-insulator-like scenario, as evinced from the T dependence of the Pauli susceptibility [19], their role as well as the impact of phonon transport are not fully disentangled and are still a matter of debate. In semiconducting materials, the phonon transport is primarily relevant and Herring [6] proposed a phenomenological

*These authors contributed equally to this work.

†Present address: Materials Science Division, Argonne National Laboratory, Lemont, Illinois 60439, USA.

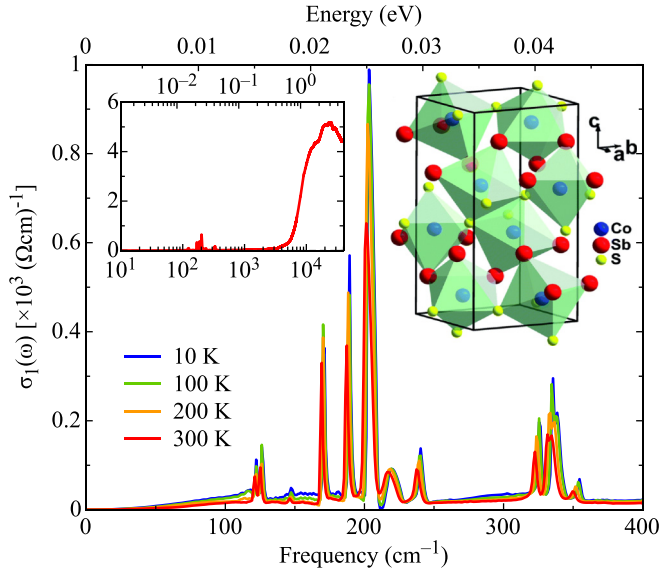


FIG. 1. Real part $\sigma_1(\omega)$ of the optical conductivity at FIR energy scales ($1 \text{ eV} = 8.06548 \times 10^3 \text{ cm}^{-1}$) at four selected T [21]. The insets show the complete spectrum at 300 K (please note the logarithmic energy scale) and the crystal structure of CoSbS [25].

approach, for which the phonon-drag component of the Seebeck coefficient is $S_{\text{ph}} \sim l_{\text{ph}} \mu_{\text{el}}^{-1}$, where l_{ph} is the phonon mean free path and μ_{el} the carrier mobility. Beyond the solely electronic (diffusionlike) contribution to S [20], enhancing l_{ph} and concomitantly reducing μ_{el} both seem of paramount relevance for novel thermoelectric materials.

Optical spectroscopy is a suitable experimental tool in order to shed light on the phonon spectrum as well as on the overall charge dynamics and thus to address the role of electron-phonon coupling. In our CoSbS single crystal, we discover very narrow infrared (IR)-active phonon modes at low T , signaling their large mean free path. Moreover, the Fano-like asymmetric shape of some of them hints at a coupling with the electronic background, due to in-gap impurity states, as revealed by a complementary scanning transmission electron microscopy study. On the other hand, the charge dynamics at high energies bears testimony to the presence of rather flat bands, as a fingerprint of massive electronic states (i.e., with low mobility). These findings support the idea that quasiballistic phonons in a correlated semiconductor pave a promising way for the realization of a high thermoelectric power at cryotemperatures.

Figure 1 highlights the T dependence of the real part $\sigma_1(\omega)$ of the optical conductivity at far-infrared (FIR) energy scales and its inset the whole absorption spectrum at 300 K [21]. We immediately recognize the insulatinglike nature of the optical response in CoSbS and the dominating IR-active phonon absorptions. The $Pbca$ (61) space group [19] of the title compound foresees a total of 27 IR-active modes (i.e., nine B_{1u} , nine B_{2u} , and nine B_{3u}). Since we are collecting the optical response with respect to the ab plane of CoSbS (right inset of Fig. 1 [25]), that number reduces to 18 (B_{2u} and B_{3u}). We clearly observe 12 distinct absorption features in $\sigma_1(\omega)$. Almost all modes are very sharp at any T and tend to get narrower and even resolution limited at low T , therefore an-

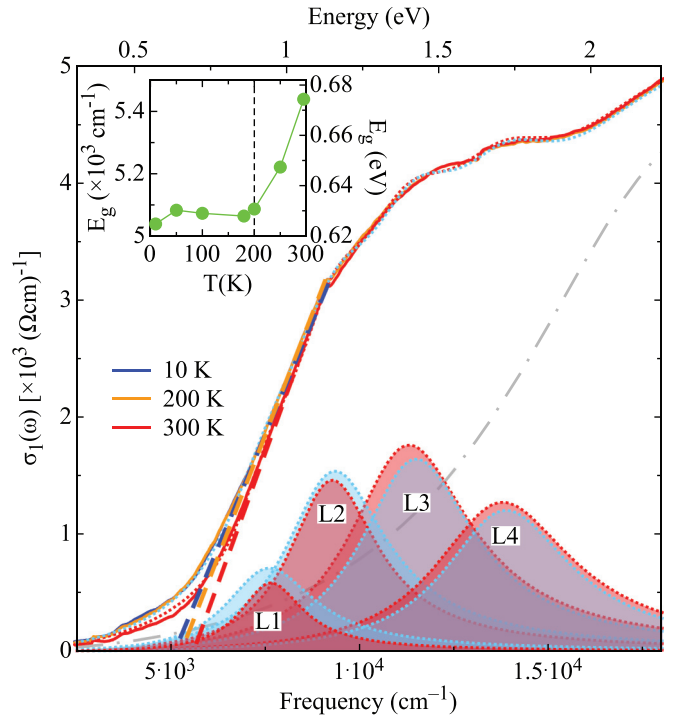


FIG. 2. Enlargement of $\sigma_1(\omega)$ at energies where the sharp absorption onset at about 5000 cm^{-1} takes place for three selected T . The intercept of the linear extrapolation (thick dashed lines) of its leading edge with the energy axis defines E_g . The inset shows its T dependence. The four harmonic oscillators (HOs), describing the gap edge, are shown at 10 and 300 K [21], thus highlighting the spectral weight [30] reshuffling between and the line-shape narrowing of the Lorentz HOs (L1–L4), pointed out in the text. Reddish and bluish colors refer to 300 and 10 K, respectively. The dotted lines are the total fits at 10 and 300 K [Eq. (S1) in the Supplemental Material (SM) [21]], while the gray dashed-dotted line is the T -independent contribution given by the additional HOs at high frequencies (Fig. S3 in SM [21]).

icipating long phonon lifetimes. Furthermore, some selected modes display an asymmetric line shape, which underlines some electron-phonon coupling similar to observations elsewhere, for instance, in graphene [26] or topological materials [27]. The implications of these latter important aspects of our data will be addressed below. Before going any further, it is worth emphasizing that the narrow gap semiconductor FeSb₂ also displays very sharp, yet mostly symmetric, phonon modes upon lowering T across the metal-insulator transition [28,29].

At higher-energy scales (inset of Fig. 1), the optical response is shaped by several interband transitions, predominantly leading to the steep onset of absorptions in $\sigma_1(\omega)$ at about 5000 cm^{-1} . Its tail then merges into the FIR background of the phonons. We associate that dominating absorption edge (Fig. 2) to excitations across the semiconducting gap (E_g), while the shallow low-frequency tail may reveal the excitations between impurity states and the conduction band edge [red and green arrows, respectively, in the DOS sketch of Fig. 3(a)]. The intercept with the frequency axis of the linear extrapolation (thick dashed lines in Fig. 2) of the absorption

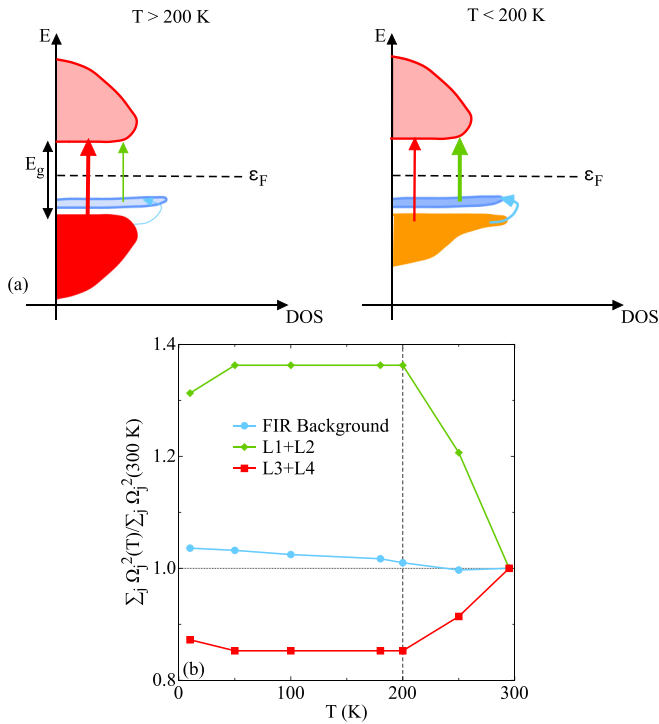


FIG. 3. (a) Proposal for the DOS evolution when crossing 200 K, with the relevant excitations (arrows) either across E_g or involving the impurity states (see text). The same color code as in (b) allows relating the excitations to their spectral weight (SW) evolution. The thickness of the arrows indeed mimics the T dependence of their relative SW changes (increasing with thickness). (b) T dependence of (total) SW, normalized at 300 K, encountered in selected components of the Lorentz phenomenological fit [30]: Electronic background at FIR energy scales (inset of Fig. S4 in SM [21]), and HOs L1 and L2 as well as L3 and L4 (Fig. 2 and Fig. S3 in SM [21]).

edge defines E_g , which displays first a fast decrease from 300 to 200 K and then it is quite constant at about 0.62 eV for $T < 200$ K (inset of Fig. 2). The magnitude of E_g is in broad agreement with values from the dc transport data in Ref. [31] as well as with its estimations from band structure calculations [32]. Interestingly enough, there are several indications that $T \sim 200$ K denotes a peculiar T crossover of this material. Indeed, two types of carriers can be clearly distinguished from the Hall resistivity and display opposite behaviors below 200 K [19]: holelike carriers with a density of about $\sim 10^{18} \text{ cm}^{-3}$ at 300 K, then increasing by several orders of magnitude at low T , and electronlike ones for which the density gets suppressed by six orders of magnitude between 200 and 2 K. Moreover, while the electron carriers keep their mobility almost unchanged at any T , the dominant hole ones display a strongly suppressed mobility below 200 K [19].

In order to further support the quantitative analysis of our data, we describe the optical response within the standard phenomenological approach based on Lorentz harmonic oscillators (HOs) [33] for the phonon FIR background and for the electronic interband transitions [Eq. (S1) in the Supplemental Material (SM) [21]]. For the phonon spectrum, we allow each phonon mode to interact with the electronic continuum [Eq. (S2) in SM [21]] via the Fano model [34].

Despite the extended amount of parameters, it is possible to extract some valuable information. For the rest of our discussion, we primarily focus our attention on the spectral weight (SW) reshuffling occurring among selected fit components as a function of T [30], as guidance for the T evolution of DOS proposed in Fig. 3(a). It is worth mentioning that an alternative, equivalent discussion of the (integrated) SW reshuffling is also proposed in Fig. S7 of SM [21]. First of all, we observe that the background at FIR energy scales gains SW by lowering T [Fig. 3(b) and Fig. S6 in SM [21]]. This signals the freezing of extrinsic carriers for $T < 200$ K into an impurity band [turquoise in Fig. 3(a)] acting as the acceptor and being located at about 30 meV above the top of the valence band [red in Fig. 3(a)], as conjectured from the dc transport properties [19]. Additional (indirect) evidence for such an electronic background and for the energy location of the impurity band will be provided below, when discussing the phonon spectrum. Second, there is an accumulation of SW at the onset of the gaplike absorption at E_g (i.e., in HOs L1 and L2), at the cost of HOs L3 and L4 [Figs. 2 and 3(b), and Fig. S5 in SM [21]] upon lowering T . The latter HOs narrow as well [Fig. 2 and Fig. S5 in SM [21]]. The resulting sharp absorption edge in $\sigma_1(\omega)$ uncovers the presence of weakly dispersive states involved in the excitations across E_g [Fig. 3(a)]. Therefore, we speculate that populating the acceptor impurity band drives the enhancement of electronic correlations in the Co $3d$ orbitals, which lead to a massive valence band [orange in Fig. 3(a)] [19,32]. Consequently, the emerging scenario from the SW reshuffling at low T in CoSbS is that of a correlated semiconductor with low μ_{el} carriers [predominantly in the valence band, Fig. 3(a)], a prerequisite for an enhanced thermopower [18,35]. Since the Seebeck coefficient decreases with magnetic field [35], we believe that spin fluctuations favor the formation of correlated states. We shall note that strong electron correlations and a sharp gap edge have been also observed in FeSb₂ [28,29,36]. The most recent optical investigation of FeSb₂ even identifies the fingerprint for a one-dimensional semiconductor [29], as a potential prerequisite for the increase of the Seebeck coefficient [37,38]. Nevertheless, this is quite unlikely in CoSbS, since it does not display typical signatures of low dimensionality in its electronic structure.

Incoherent high-resolution scanning transmission electron microscopy (STEM) is rather instrumental in order to probe the existence of structural defects, as the possible origin of the impurity states. For our STEM measurements [21] we use the high-angle annular-dark-field (HAADF) imaging mode, under which the image intensity of atomic columns is approximately proportional to $Z^{1.7}$, where Z is the atomic number. Figure 4(a) shows a STEM-HAADF image from the CoSbS single crystal viewed along the [001] direction (i.e., c axis in the right inset of Fig. 1) with a convergent angle of 21 mrad and a collection angle from 67 to 275 mrad. The atomic arrangement based on the observed image contrast agrees with the $Pbca$ symmetry of the CoSbS structure [19], as shown in the magnified image [Fig. 4(b)] where the [001] projected CoSbS unit cell (right inset of Fig. 1) is embedded. The heavy Sb atoms are clearly seen as bright dots, while the Co and S atoms, in the vicinity of the Sb atoms, have very weak contrast and are shown as tails of the Sb columns, due to

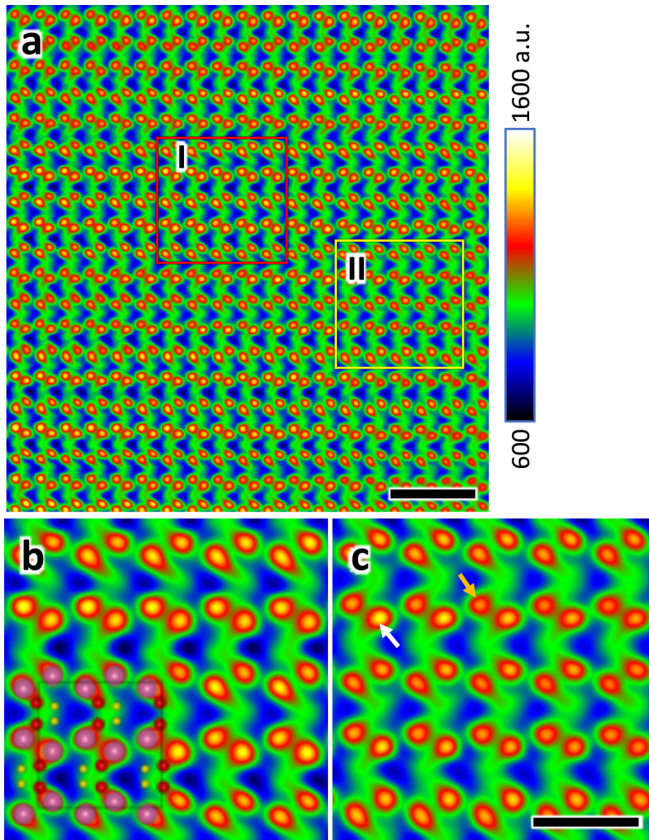


FIG. 4. (a) High-resolution STEM image recorded on a HAADF detector with the incident beam along the [001] direction of the CoSbS single crystal. The image is filtered in frequency space by applying a periodic mask to remove the noise. Scale bar: 1 nm. (b), (c) Magnified images from areas I and II marked by rectangles in (a) are shown in (b) and (c), respectively. Scale bar: 0.5 nm. The [001] projection of the structure model (right inset of Fig. 1) is embedded in (b) with wine, red, and yellow spheres representing Sb, Co, and S, respectively. Overall, the image intensity of Sb columns in (c) is weaker than that in (b), especially at the atomic positions marked by the white and orange arrows, implying relative changes in the Sb occupancy. The color scale, shown on the right, is used for the intensity of the image in all panels.

their low atomic weight. Overall, the crystal does not display any dislocations or twin formation, which would change the average structure and lattice parameters [21]. However, a close inspection reveals that the peak intensity of the Sb column varies slightly, as shown in Fig. 4(c) where the peak intensity indicated by the white arrow is higher than that by the orange arrow. The change of the relative intensity of the projected atomic images [Figs. 4(a)–4(c)] may be consistent with either Sb vacancies or Sb interstitial defects within the Sb atomic columns [Figs. S12(a)–S12(c) in SM [21]]. Within an ionic picture, the negative Sb valency in CoSbS in combination

with the need for acceptor states in order to account for the optical and dc transport results calls for the latter possibility [Fig. S12(d) in SM [21]]. By comparing the image simulations with the experimental image [Fig. S12 in SM [21]], we estimate that the relative change of the Sb occupancy varies within 5% from column to column. Interestingly enough, Sb point-defect control of thermoelectricity was recently achieved in FeSb₂, via the generation of (donorlike) in-gap states [39].

Finally, we turn our attention again to the phonon modes, which are rather illuminating towards our understanding of the peculiar intrinsic thermoelectric properties. The small phonon linewidths in CoSbS [Fig. S11(a) in SM [21]] are comparable to those discovered in the optical response of FeSb₂ [28,29], for which a quasiballistic phonon regime was advanced [29]. Indeed, this concomitantly pairs with the long phonon mean free path, derived from the FeSb₂ thermal conductivity with Fourier's law [18]. Therefore, we may argue that CoSbS is equally characterized by coherent phonons [40], consistent with a phonon-drag mechanism as the origin for the enhancement of S_{ph} [18]. Furthermore, our data on CoSbS provide evidence for asymmetric phonon modes, as deployed by the Fano q_i parameter [21,34]. In fact, $1/q_i$ [Fig. S11(b) of SM [21]] is different from zero (i.e., symmetric line shape), either negative or positive, for the IR-active phonons between 200 and 225 cm^{-1} (i.e., Ph7 and 8 in Fig. S4 of SM [21]). This finding bears testimony to some electron-phonon coupling, further revealing the presence of an electronic background at those FIR energy scales (~ 30 meV), as pointed out above. This could even suggest that a charged-phonon effect [41] takes place, complementary to the phonon drag model. Again, CoSbS differentiates from FeSb₂, since contrasting reports with respect to the existence of an electron-phonon coupling appeared in the literature [28,29]. Asymmetric phonon modes were only discovered in the early optical data of FeSb₂ [28].

In conclusion, the optical properties of CoSbS at low T signal the important role of coherent phonons (i.e., large l_{ph}) and heavy (i.e., low μ_{el}) carriers, both being an asset for the enhancement of $S_{\text{ph}} \sim l_{\text{ph}}\mu_{\text{el}}^{-1}$ [6]. This mixture of ingredients from the lattice dynamics and the electronic band structure turns out to be essential in order to enhance the thermopower at cryotemperatures [42]. The binding aspect for such a mixture in the correlated semiconductor CoSbS is given by the presence of in-gap impurity states, originating from interstitial Sb, which seem to play quite a decisive role. Our data therefore propose the selective tuning of impurity states as an affordable strategy towards the enhancement of thermoelectric power.

The authors thank C.C. Homes for fruitful discussions. Work at Brookhaven National Laboratory was supported by the US Department of Energy, Office of Basic Energy Science, Division of Materials Science and Engineering, under Contract No. DE-SC0012704.

[1] X. Zhang and L.-D. Zhao, *J. Materiomics* **1**, 92 (2015).

[2] G. J. Snyder and E. S. Toberer, Complex thermoelectric materials, in *Materials for Sustainable Energy*, edited by V. Dusastre (World Scientific, Singapore, 2010), pp. 101–110.

[3] J. He, M. G. Kanatzidis, and V. P. Dravid, *Mater. Today* **16**, 166 (2013).

[4] L. Wu, Q. Meng, C. Jooss, J.-C. Zheng, H. Inada, D. Su, Q. Li, and Y. Zhu, *Adv. Funct. Mater.* **23**, 5728 (2013).

- [5] N. W. Ashcroft and N. D. Mermin, *Solid State Physics* (Holt-Saunders, Philadelphia, 1976).
- [6] C. Herring, *Phys. Rev.* **96**, 1163 (1954).
- [7] T. H. Geballe and G. W. Hull, *Phys. Rev.* **94**, 1134 (1954).
- [8] G. Xie, D. Ding, and G. Zhang, *Adv. Phys.: X* **3**, 1480417 (2018).
- [9] Y. Matsushita, H. Bluhm, T. H. Geballe, and I. R. Fisher, *Phys. Rev. Lett.* **94**, 157002 (2005).
- [10] Y. Matsushita, P. A. Wianeci, A. T. Sommer, T. H. Geballe, and I. R. Fisher, *Phys. Rev. B* **74**, 134512 (2006).
- [11] A. Pal, M. Chinotti, L. Degiorgi, P. Walmsley, and I. R. Fisher, *Phys. Rev. Materials* **3**, 054801 (2019).
- [12] P. Giraldo-Gallo, P. Walmsley, B. Sangiorgio, S. C. Riggs, R. D. McDonald, L. Buchauer, B. Fauqué, C. Liu, N. A. Spaldin, A. Kaminski, K. Behnia, and I. R. Fisher, *Phys. Rev. Lett.* **121**, 207001 (2018).
- [13] P. Walmsley, C. Liu, A. D. Palczewski, P. Giraldo-Gallo, C. G. Olson, I. R. Fisher, and A. Kaminski, *Phys. Rev. B* **98**, 184506 (2018).
- [14] M. Dzero and J. Schmalian, *Phys. Rev. Lett.* **94**, 157003 (2005).
- [15] G. D. Mahan and J. O. Sofo, *Proc. Natl. Acad. Sci. USA* **93**, 7436 (1996).
- [16] A. Bentien, S. Johnsen, G. K. H. Madsen, B. B. Iversen, and F. Steglich, *Europhys. Lett.* **80**, 17008 (2007).
- [17] P. Sun, W. Xu, J. M. Tomczak, G. Kotliar, M. Søndergaard, B. B. Iversen, and F. Steglich, *Phys. Rev. B* **88**, 245203 (2013).
- [18] H. Takahashi, R. Okazaki, S. Ishiwata, H. Taniguchi, A. Okutani, M. Hagiwara, and I. Terasaki, *Nat. Commun.* **7**, 12732 (2016).
- [19] Q. Du, M. Abeykoon, Y. Liu, G. Kotliar, and C. Petrovic, *Phys. Rev. Lett.* **123**, 076602 (2019).
- [20] H. Fritzsche, *Solid State Commun.* **9**, 1813 (1971).
- [21] See Supplemental Material at <http://link.aps.org/supplemental/10.1103/PhysRevB.103.L161111> for additional information on the sample growth, experimental techniques, and data analysis, which includes Refs. [22–24].
- [22] E. J. Kirkland, *Advanced Computing in Electron Microscopy* (Plenum, New York, 1998).
- [23] J. M. LeBeau, S. D. Findlay, L. J. Allen, and S. Stemmer, *Nano Lett.* **10**, 4405 (2010).
- [24] The spectral weight (SW) of the optical conductivity corresponds to its integral $SW(T) = \frac{Z_0}{\pi^2} \int_{\omega_1}^{\omega_2} \sigma_1(\omega'; T) d\omega'$, expressed in units of cm^{-2} [33]. ω_i ($i = 1$ and 2) define the energy interval, relevant for the SW estimation.
- [25] Y. You, X. Su, S. Hao, W. Liu, Y. Yan, T. Zhang, M. Zhang, C. Wolverton, M. G. Kanatzidis, and X. Tang, *J. Mater. Chem. A* **6**, 15123 (2018).
- [26] Z. Li, C. H. Lui, E. Cappelluti, L. Benfatto, K. F. Mak, G. L. Carr, J. Shan, and T. F. Heinz, *Phys. Rev. Lett.* **108**, 156801 (2012).
- [27] B. Xu, Y. M. Dai, L. X. Zhao, K. Wang, R. Yang, W. Zhang, J. Y. Liu, H. Xiao, G. F. Chen, S. A. Trugman, J.-X. Zhu, A. J. Taylor, D. A. Yarotski, R. P. Prasankumar, and X. G. Qiu, *Nat. Commun.* **8**, 14933 (2017).
- [28] A. Perucchi, L. Degiorgi, R. Hu, C. Petrovic, and V. F. Mitrović, *Eur. Phys. J. B* **54**, 175 (2006).
- [29] C. C. Homes, Q. Du, C. Petrovic, W. H. Brito, S. Choi, and G. Kotliar, *Sci. Rep.* **8**, 11692 (2018).
- [30] Within the Lorentz phenomenological approach [21], the spectral weight (SW) of each component corresponds to the square of the (Lorentz) harmonic oscillator (HO) strength.
- [31] Y. You, X. Su, W. Liu, Y. Yan, T. Hu, C. Uher, and X. Tang, *RSC Adv.* **7**, 34466 (2017).
- [32] D. Parker, A. F. May, H. Wang, M. A. McGuire, B. C. Sales, and D. J. Singh, *Phys. Rev. B* **87**, 045205 (2013).
- [33] M. Dressel and G. Gruner, *Electrodynamics of Solids* (Cambridge University Press, Cambridge, UK, 2002).
- [34] U. Fano, *Phys. Rev.* **124**, 1866 (1961).
- [35] R. Gupta and C. Bera, *Phys. Rev. B* **101**, 155206 (2020).
- [36] A. Herzog, M. Marutzky, J. Sichelschmidt, F. Steglich, S. Kimura, S. Johnsen, and B. B. Iversen, *Phys. Rev. B* **82**, 245205 (2010).
- [37] L. D. Hicks and M. S. Dresselhaus, *Phys. Rev. B* **47**, 16631(R) (1993).
- [38] J.-S. Rhyee, K. H. Lee, S. M. Lee, E. Cho, S. I. Kim, E. Lee, Y. S. Kwon, J. H. Shim, and G. Kotliar, *Nature (London)* **459**, 965 (2009).
- [39] Q. Du, L. Wu, H. Cao, C.-J. Kang, C. Nelson, G. L. Pascut, T. Besara, K. Haule, G. Kotliar, I. Zaliznyak, Y. Zhu, and C. Petrovic, *npj Quantum Mater.* **6**, 13 (2021).
- [40] The mean free path is calculated as $l_{\text{ph}} = v\tau_{\text{ph}}$, where $\tau_{\text{ph}} \sim 1/\gamma$ is the relaxation time, inversely proportional to the phonon linewidth γ and $v = 3700$ m/s is the sound velocity [19]. For the sake of arguments we use here the sound velocity instead of the group one for optical (transverse) phonons. The phonon linewidth is equal to the damping of the Fano-like mode [Eq. (S2) in SM [21]]. Similarly to FeSb₂ [29], we obtain values of l_{ph} comparable to several tens of the lattice constants.
- [41] E. Cappelluti, L. Benfatto, M. Manzardo, and A. B. Kuzmenko, *Phys. Rev. B* **86**, 115439 (2012).
- [42] M. Battiato, J. M. Tomczak, Z. Zhong, and K. Held, *Phys. Rev. Lett.* **114**, 236603 (2015).